Journal of Power Sources, 43–44 (1993) 289–300

The versatility of MnO_2 for lithium battery applications

M. M. Thackeray, M. H. Rossouw, A. de Kock, A. P. de la Harpe,
R. J. Gummow, K. Pearce and D. C. Liles
Division of Materials Science and Technology, CSIR, P.O. Box 395, Pretoria 0001 (South Africa)

Abstract

Manganese dioxide has for many years found widespread use as a cathode material in aqueous Leclanché, zinc chloride and alkaline cells and, more recently, in nonaqueous lithium cells. However, despite the large number of polymorphic structures that exist in the manganese dioxide family, the battery industry has used γ-MnO_2 exclusively as the positive electrode in these cells. With the advent of rechargeable lithium battery technology, research efforts have demonstrated that other MnO_2 structures, when processed in the correct way, provide attractive electrochemical properties for lithium cells. In this paper, some recent advances that have been made in MnO_2 materials technology are discussed, for example, in the development of α-MnO_2, layered-MnO_2, spinel-related $Li_2O \cdot yMnO_2$ ($y \geqslant 2.5$) and ramsdellite-MnO_2 materials. An attempt has been made to clarify issues relating to the structural features of 'CDMO'-type materials that are prepared by the reaction of γ-MnO_2 with $LiNO_3$ (or LiOH) at 300–400 °C.

Introduction

Recent international research on cathode materials for ambient temperature rechargeable lithium batteries has been focused largely on the evaluation of the Li-insertion compounds Li_xCoO_2, Li_xNiO_2 and $Li_xMn_2O_4$ ($0 < x \leqslant 1$) for 4 V systems [1–3] and a variety of MnO_2-based materials for 3 V systems [4–9]. Of these materials, the manganese oxides are particularly attractive because they are relatively cheap and non-toxic. Moreover, the MnO_2 system is an extremely versatile one as demonstrated in Table 1. This system therefore offers the possibility of tailor-making an electrode

TABLE 1

Examples of MnO_2 compounds

MnO_2 type	Structure type	Interstitial space of the MnO_2 structure
α-MnO_2	Hollandite	(1×1) and (2×2) tunnels
β-MnO_2	Rutile	(1×1) tunnels
γ-MnO_2	Intergrowth of rutile/ramsdellite[a]	(1×1) and (1×2) tunnels
δ-MnO_2	Layered (hydrated)	layers of H_2O and stabilising cations
λ-MnO_2	Spinel	3-dimensional network of channels
$Li_2O \cdot yMnO_2$ ($y \geqslant 2.5$)	Spinel	
CDMO (Li:Mn = 3:7)	Domains of lithiated γ-MnO_2 and spinel[a]	refer to features above for γ-MnO_2 and spinel phases

[a]The amount of a particular phase present is dependent on the processing temperature.

0378-7753/93/$6.00

structure with the required electrochemical properties. In the search for an optimum rechargeable electrode, the approach at the CSIR, South Africa, over the past few years has been to synthesise a wide range of anhydrous MnO_2-based materials from various precursors and to evaluate their electrochemical activity in Li cells. This research effort has produced several materials of high purity with novel or modified structures.

Recent progress that has been made in characterising the structural and electrochemical properties of some of these materials is summarised in this paper. Particular attention has been given to ramsdellite-MnO_2 and to the current debate on the structure of composite dimensional manganese oxide (CDMO) products that are synthesised typically by the reaction of LiOH (or $LiNO_3$) with γ-MnO_2 (Li:Mn = 3:7) at 300–400 °C.

Discussion

α-MnO_2

Recent studies have shown that acid leaching of Li_2O from the Li_2MnO_3 rock-salt structure at ~90 °C causes a phase transition to a highly-crystalline hydrated α-MnO_2 product with the composition α-$MnO_2 \cdot 0.3H_2O$ [6]. Moreover, it was reported that the product could be almost entirely dehydrated at 300 °C, leaving a virtually pure α-MnO_2 structure. This finding dispels the common belief that α-MnO_2 structures have to be stabilised by foreign cations at the centre of the relatively large (2×2) channels to prevent a structural collapse [10].

Initial investigations have shown that this α-MnO_2 product shows promise as a cathode material for room-temperature Li cells [6]. The open-circuit voltage (OCV) versus composition curve in Fig. 1 demonstrates that one Li^+ ion can be introduced into the structure over the voltage range 3.8 to 2.0 V versus pure Li. When discharged

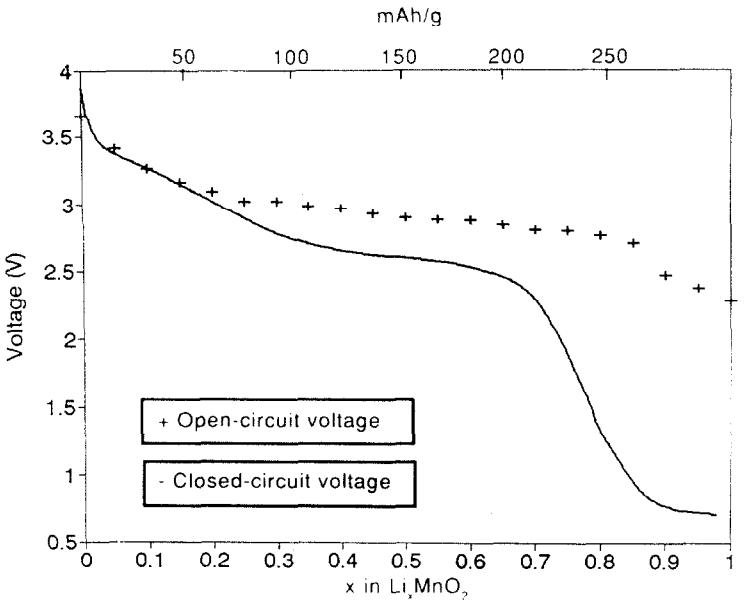

Fig. 1. Open-circuit voltage and closed-circuit voltage data for a Li/α-MnO_2 cell.

at a continuous current rate of 0.2 mA/cm^2 in flooded electrolyte prismatic cells, an initial discharge capacity of 230 mA h/g can be achieved to a 2 V cutoff voltage. Cyclic voltammetry data indicate that Li is inserted into the structure in a two-stage process and that the process is reversible [6]. Because the narrow (1×1) channels in the structure are energetically unfavourable for accommodating a significant quantity of Li, it is believed that most of the inserted Li is accommodated in the (2×2) channels.

Although the rechargeability of this product is still to be fully investigated, it is worthwhile to note that the rechargeability of α-MnO_2 electrodes that contain cations such as K^+ and NH_4^+ in the (2×2) channels can be significantly improved if the foreign cations are ion-exchanged by Li^+ at 300 °C [5].

Layered MnO_2

Although a $LiMnO_2$ compound, isostructural with layered $LiCoO_2$, has not yet been synthesised, recent reports suggest that it is possible to synthesise a layered-type MnO_2 compound by leaching out Li_2O with acid from the layered Li_2MnO_3 rock-salt structure at 25 °C [8] according to the reaction:

$$Li_2MnO_3 \xrightarrow{\text{acid}} Li_{2-2x}MnO_{3-x} + xLi_2O \quad (0 < x \leqslant 1) \tag{1}$$

The resulting $Li_{2-2x}MnO_{3-x}$ structures contain some residual Li^+ ions and ion-exchanged H^+ ions.

Extensively delithiated $Li_{2-2x}MnO_{3-x}$ layered compounds are thermally unstable and transform to a γ/β-MnO_2 structure when heated at 300 °C. Delithiated $Li_{2-2x}MnO_{3-x}$ samples that contain an appreciable quantity of Li transform at 300 °C to a product containing domains of Li_2MnO_3 and spinel-related structures in the system $Li_xMn_{2-z}O_4$ ($0 \leqslant x \leqslant 4/3$, $0 \leqslant z \leqslant 1/3$); in the spinel-related structures the ratio of Mn ions in alternate layers may deviate slightly from the ideal 3:1 ratio.

Layered-MnO_2 electrodes heated at 100 °C to remove surface water have been shown to deliver capacities in excess of 200 mA h/g on the initial discharge in Li cells; the capacity drops steadily on cycling. The capacity loss has been attributed largely to some residual water still associated with the structure [8]. Further improvements in the rechargeability of this material can, however, be expected.

The spinel system $Li_2O \cdot yMnO_2$ ($y \geqslant 2.5$)

The spinel system $Li_2O \cdot yMnO_2$ ($y \geqslant 2.5$) is a subset of the spinel solid-solution system $Li_xMn_{2-z}O_4$ ($0 \leqslant x \leqslant 4/3$, $0 \leqslant z \leqslant 1/3$) which is defined by the λ-MnO_2–$Li_4Mn_5O_{12}$–$LiMn_2O_4$ tie triangle in the Li–Mn–O phase diagram [9]. Table 2 gives the cation arrangement, in spinel notation, of four selected compounds in the

TABLE 2

Spinel and defect spinels in the system $Li_2O \cdot yMnO_2$ ($y \geqslant 2.5$)

Compound	y	Spinel notation	Theoretical capacity (mA h/g)
$Li_4Mn_5O_{12}$	2.5	$Li[Mn_{1.67}Li_{0.33}]O_4$	163
$Li_2Mn_3O_7$	3.0	$Li_{0.85}\square_{0.15}[Mn_{1.71}Li_{0.29}]O_4$	184
$Li_2Mn_4O_9$	4.0	$Li_{0.89}\square_{0.11}[Mn_{1.88}\square_{0.22}]O_4$	213
λ-MnO_2	∞	$\square_{1.0}[Mn_2]O_4$	308

$Li_2O \cdot yMnO_2$ system and their theoretical discharge capacity when discharged to a rock-salt stoichiometry. A particularly attractive feature of the spinel system is that the $[Mn_{2-z}]O_4$ framework provides a stable 3-dimensional network for Li^+ ion transport.

Li/λ-MnO_2 cells discharge at approximately 4 V versus pure Li in two distinct stages for the range $0 < x < 0.5$ in Li_xMnO_2 [3, 11], and at approximately 3 V for the range $0.5 \leqslant x \leqslant 1.0$ [12]. Li/λ-MnO_2 cells have been well-characterised and will not be discussed further in this paper. The $Li_2O \cdot yMnO_2$ spinels ($2.5 \leqslant y \leqslant 4.0$) which, like λ-$MnO_2$, contain tetravalent manganese, discharge almost all their capacity at 3 V versus pure Li [9]. $Li_4Mn_5O_{12}$ and $Li_2Mn_4O_9$ cathodes can deliver steady capacities in excess of 150 mA h/g, respectively, at least for the initial cycles (Fig. 2(a) and (b)). The good rechargeability and stability of these spinel cathodes are attributed to the

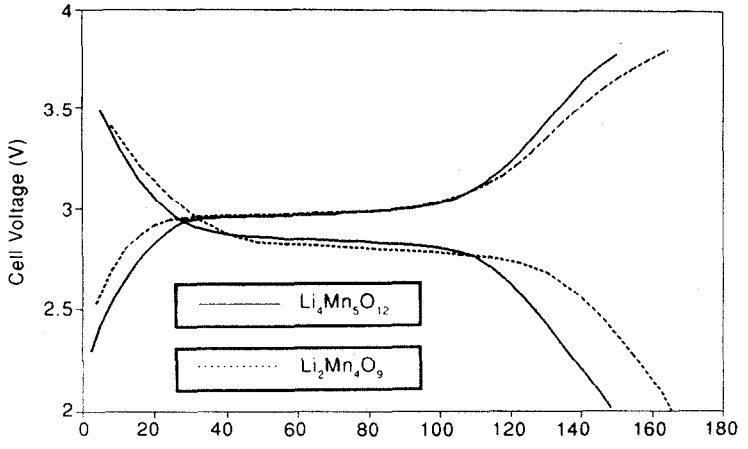

(a)

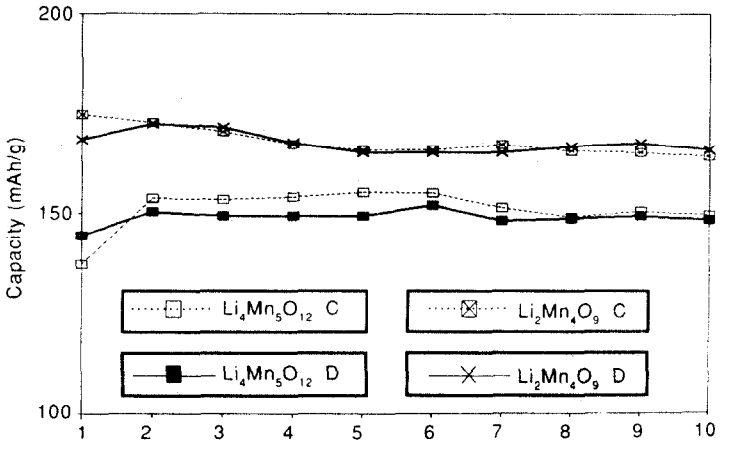

(b)

Fig. 2. (a) Typical charge/discharge profiles of Li/$Li_4Mn_5O_{12}$ and Li/$Li_2Mn_4O_9$ cells; charge current: 0.2 mA/cm^2, and discharge current: 0.4 mA/cm^2. (b) Variation of cathode capacity with cycle number of Li/$Li_4Mn_5O_{12}$ and Li/$Li_2Mn_4O_9$ cells. C = charge, D = discharge.

fact that Li is inserted into a cubic structure with a minimal expansion of the unit cell over a wide compositional range [9]. The onset of a Jahn–Teller distortion that is induced into the cathode structure when the manganese oxidation state reaches ~3.5 and that transforms the symmetry of the cubic unit cell to tetragonal symmetry, occurs late in the discharge reaction. This distortion is generally associated with a 5 to 6% increase in volume of the unit cell and may harm the rechargeability of the electrode if discharged too deeply. In $Li_{1+x}Mn_2O_4$ cathodes, the onset of the Jahn–Teller distortion takes place almost immediately, at $x \approx 0.08$, and is therefore probably the reason why $Li/Li_{1+x}Mn_2O_4$ cells exhibit an inferior cycling behaviour compared with $Li/Li_2O \cdot yMnO_2$ cells.

Spinel materials in the system $Li_2O \cdot yMnO_2$ ($2.5 \leqslant y \leqslant 4.0$) can be readily manufactured within a few hours by the solid-state reaction in air of $MnCO_3$ with LiOH (or Li_2CO_3) at moderate temperatures, for example 300–400 °C, as shown by the X-ray diffraction patterns in Fig. 3(a)–(d) [9]. This reaction involves the decomposition of the precursor materials and a construction of the spinel framework – a process during which, under carefully-controlled conditions, the Mn^{2+} ions are fully oxidised to Mn^{4+}. These reactions demonstrate, unequivocally, that at these temperatures the formation of Li–Mn–O spinel phases is thermodynamically favoured over other structure types, particularly when the Li:Mn ratio in the starting mixture is in the range 1:1.2 to 1:2.0. The cation arrangements in $Li_2Mn_3O_7$ [13], $Li_2Mn_4O_9$ [14] and λ-MnO_2 [15] in Table 2 have been determined by neutron diffraction analyses.

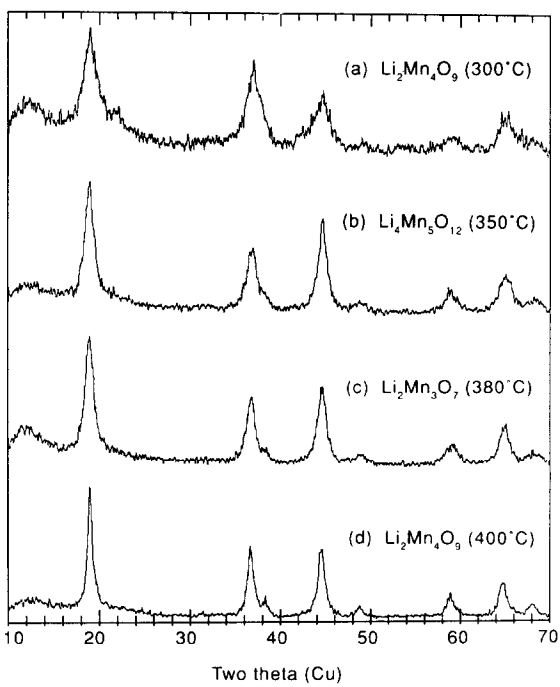

Fig. 3. Powder X-ray diffraction patterns of: (a) $Li_2Mn_4O_9$ (300 °C), (b) $Li_4Mn_5O_{12}$ (350 °C), (c) $Li_2Mn_3O_7$ (380 °C), and (d) $Li_2Mn_4O_9$ (400 °C). The spinel phases may be slightly oxygen deficient, particularly when synthesised at the lower temperatures. In (a) there is evidence of a minor amount of a lithiated γ-MnO_2 phase.

If, in the above experiments, the $MnCO_3$ precursor is replaced by γ-MnO_2 (either chemical manganese dioxide (CMD) or electrolytic manganese dioxide (EMD) which tend to be oxygen-deficient materials with a typical stoichiometry $MnO_{\sim 1.9}$), the reaction with LiOH at 300–400 °C (20 h) yields a product that consists essentially of domains of a lithiated γ-MnO_2 phase of approximate composition $Li_{0.2}MnO_{1.9+x}$ ($0 \leqslant x \leqslant 0.2$) [16–18] and a predominant spinel phase in the system $Li_xMn_{2-z}O_4$ ($0 \leqslant x \leqslant 4/3$, $0 \leqslant z \leqslant 1/3$) [9]. The X-ray diffraction patterns of various products are shown in Fig. 4(a)–(e). The reaction is more sluggish than when $MnCO_3$ is used as a precursor because Li_2O must be incorporated into a fully oxidised (or almost fully-oxidised) MnO_2 structure. When the Li:Mn ratio in the starting material is 1:2, and if all the LiOH is consumed in the reaction, the process on full oxidation of the products can, in principle, be represented by a variety of reactions, for example:

$$LiOH + 2MnO_{1.9} \xrightarrow{0.1O_2} 0.71Li_{0.2}MnO_{2.1}(\gamma) + 0.43Li_2Mn_3O_7(\text{spinel}) + 0.5H_2O \quad (2)$$

or

$$LiOH + 2MnO_{1.9} \xrightarrow{0.1O_2} Li_{0.2}MnO_{2.1}(\gamma) + 0.2Li_4Mn_5O_{12}(\text{spinel}) + 0.5H_2O \quad (3)$$

In reaction (2), 36% of the electrochemically-active MnO_2 component is contained in the γ-phase and 64% in the spinel phase, whereas in reaction (3) 50% of the MnO_2 is in the γ-phase and 50% in the spinel phase.

As the processing temperature is raised to 400 °C, the concentration of the spinel component in the product increases at the expense of the $Li_{0.2}MnO_{2+x}(\gamma)$ phase, as

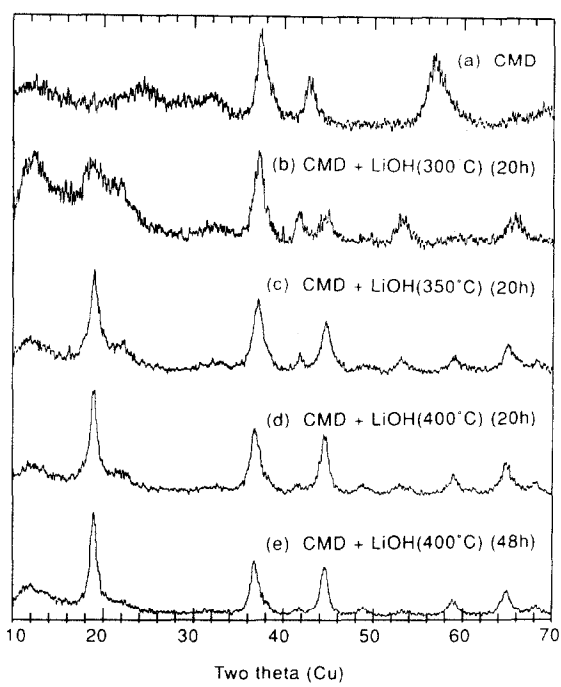

Fig. 4. Powder X-ray diffraction patterns of the reaction products of CMD and LiOH (Li:Mn = 1:2) at various temperatures: (a) a CMD precursor, (b) 300 °C (20 h), (c) 350 °C (20 h), (d) 400 °C (20 h), and (e) 400 °C (48 h).

expected, because of the predominant stability of the spinel phase in the 300–400 °C temperature range; the composition of the spinel component changes as the temperature is increased. After a 48 h soak at 400 °C, an essentially single-phase $Li_2Mn_4O_9$ product is formed (Fig. 4(e)) according to the reaction:

$$LiOH + 2MnO_{1.9} \xrightarrow{0.1O_2} 0.5Li_2Mn_4O_9 + 0.5H_2O \quad (4)$$

In practice it is not easy to utilise all the Li salt in the reaction or to fully oxidise the lithiated γ-MnO_2 and spinel phases, particularly when short reaction times and lower temperatures are used. The degree of oxidation of the final product and the ratio of spinel to lithiated γ-MnO_2 phase are also dependent on the value of x in MnO_x, the oxygen partial pressure and on the lithium compound used, for example, $LiNO_3$ or LiOH.

It should be noted that an alternative reaction would be:

$$LiOH + 2MnO_{1.9} \xrightarrow{0.1O_2} 1.67Li_{0.2}MnO_{2.1}(\gamma) + 0.33Li_2MnO_3(\text{rock salt}) + 0.5H_2O \quad (5)$$

In this reaction, 83% of the MnO_2 is contained in the γ-phase and only 17% in the rock-salt phase. However, it is believed that reaction (5) is not significant for reasons outlined later in the sections on ramsdellite MnO_2 and 'CDMO' materials.

Ramsdellite MnO_2

γ-MnO_2 materials (whether EMD or CMD) contain domains of intergrown β-MnO_2 and ramsdellite MnO_2; they are, in general, poorly crystalline. A high concentration of β-MnO_2 in the structure impairs the performance of γ-MnO_2 electrodes because the narrow (1×1) channels in β-MnO_2 can accommodate only $0.2Li^+$ ions per formula unit [19]. It would therefore seem advantageous to prepare an anhydrous γ-MnO_2 electrode structure with a very high concentration of ramsdellite domains (hereafter referred to as R-MnO_2 for convenience) which, with larger (2×1) channels, can accommodate significantly more Li than β-MnO_2.

A highly-crystalline R-MnO_2 phase has recently been synthesised by acid digestion of the spinel $Li_2Mn_4O_9$ at 95 °C [20] according to the reaction:

$$Li_2Mn_4O_9(\text{spinel}) \underset{\text{air (300–400 °C)}}{\overset{\text{acid (95 °C)}}{\rightleftharpoons}} 4MnO_2(\text{ramsdellite}) + Li_2O \quad (6)$$

The spinel-ramsdellite transition is reversible, but anhydrous conditions and higher temperatures are required to accomplish the reaction in the reverse direction. The existence of the crystalline R-MnO_2 phase has made it possible to gather valuable information about the structural changes that occur during discharge of Li/γ-MnO_2 cells. A lithiated product of composition $Li_{0.5}MnO_2$ was obtained by reaction of R-MnO_2 with a slight excess of n-butyllithium at 25 °C. Specific details about sample preparation and procedures for the structure refinement of these phases will be reported elsewhere.

The X-ray diffraction patterns of R-MnO_2 and its chemically-lithiated product $Li_{0.5}MnO_2$ are shown in Fig. 5(a) and (b). The structures of R-MnO_2 and $Li_{0.5}MnO_2$ as determined by profile refinement of the X-ray diffraction data are illustrated in Fig. 6(a) and (b), respectively. The lattice constants of the orthorhombic unit cell (Pnam) of R-MnO_2, $a = 9.38$ Å, $b = 4.47$ Å and $c = 2.85$ Å, are in good agreement with literature values [21]. Refinement of this structure indicated that there was a small amount (<10%) of manganese in the (2×1) channels. A minor concentration of intergrown β-MnO_2 in the R-MnO_2 structure can therefore not be discounted.

The structure of the lithiated product (Fig. 6(b)) shows that Li insertion into R-MnO_2 causes a buckling of the hexagonally-close-packed layers and a transformation

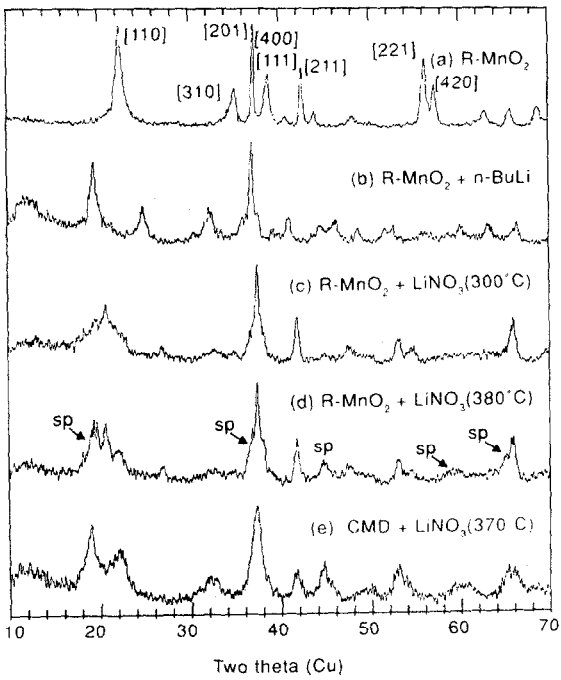

Fig. 5. Powder X-ray diffraction patterns of: (a) R-MnO_2, (b) $Li_{0.5}MnO_2$ from R-MnO_2 and n-butyllithium, (c) the reaction product of R-MnO_2+$LiNO_3$ (Li:Mn=3:7) at 300 °C, (d) same as (c) but at 380 °C. Spinel peaks are denoted sp., (e) reaction product of CMD+$LiNO_3$ (Li:Mn=3:7) at 370 °C.

towards a cubic-close-packed structure in response to an increase of electrostatic interactions between the inserted Li ions and manganese ions in neighbouring face-shared octahedra. The refined lattice parameters of the lithiated phase are a= 9.55 Å, b=5.06 Å and c=2.85 Å. The volume of the unit cell is 15.4% larger than that of the parent compound. It is anticipated that on complete lithiation of R-MnO_2, the final $LiMnO_2$ product would have a rock-salt structure with a distorted cubic-close-packed oxygen array as opposed to a NiAs-type structure in which the anions are hexagonally-close-packed, as previously suggested [22].

The discharge profiles of a Li/R-MnO_2 cell on closed-circuit and open-circuit are given in Fig. 7. The discharge profile of the Li/R-MnO_2 cell obtained at a continuous drain of 0.2 mA/cm^2 indicates that the R-MnO_2 electrode delivers 222 mA h/g on the initial discharge to a 2.5 V cutoff voltage. The OCV versus composition plot indicates that one Li is inserted into the structure over the voltage range 3.72–2.81 V. The single-phase process that occurs for the range $0 \leqslant x \leqslant 0.25$ is of particular significance. It suggests that the R-MnO_2 phase incorporates $0.25Li^+$ ions within its structure before Li^+–$Mn^{4+/3+}$ electrostatic interactions induce the buckling of the oxygen planes. This distortion is responsible for significant changes to the X-ray diffraction pattern of lithiated γ-MnO_2 products, for example, a major shift of the [110] peak at 22.2° 2θ to a lower 2θ value (19° 2θ), and the shift of the doublet [221] and [420] peaks between 56°–57° 2θ to 52°–53° 2θ.

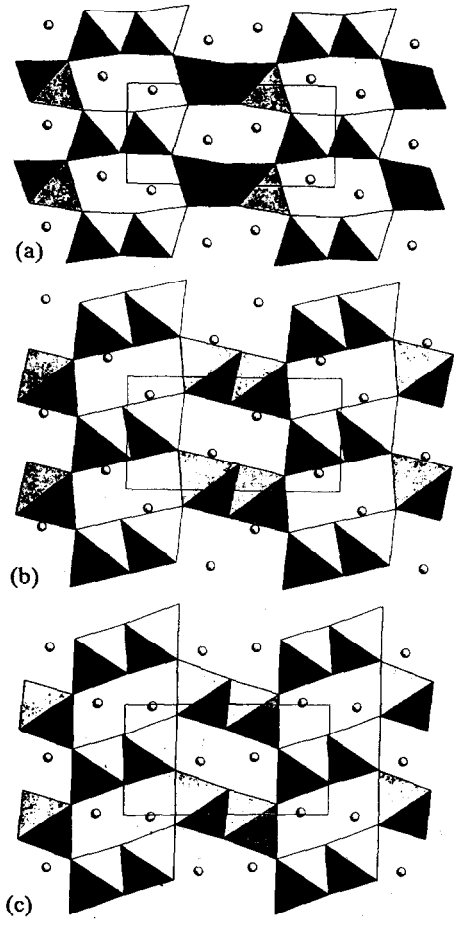

Fig. 6. The structures of: (a) R-MnO_2, (b) $Li_{0.5}MnO_2$ from R-MnO_2 and n-butyllithium, and (c) lithiated R-MnO_2 from R-MnO_2 and $LiNO_3$ at 300 °C, as determined from powder X-ray diffraction data [20]. The ○ in the (2×1) channels represent a small amount (<10%) of Mn.

The reaction of R-MnO_2 with $LiNO_3$ at 300 and 380 °C

The X-ray diffraction patterns of R-MnO_2 after reaction with $LiNO_3$ (Li:Mn = 3:7) at 300 and 380 °C in air are shown in Fig. 5(c) and (d).

at 300 °C

The X-ray diffraction pattern of the product formed at 300 °C provided the following information:

(i) The dominant phase present was a lithiated R-MnO_2 product with an orthorhombic unit cell $a = 9.27$ Å, $b = 4.97$ Å and $c = 2.86$ Å. This represents a 10.4% volume increase of the parent unit cell.

(ii) The weak peak at ~45° 2θ and the asymmetry of the [110] reflection towards lower 2θ that showed an additional peak at ~19° 2θ were attributed to the onset of spinel-formation.

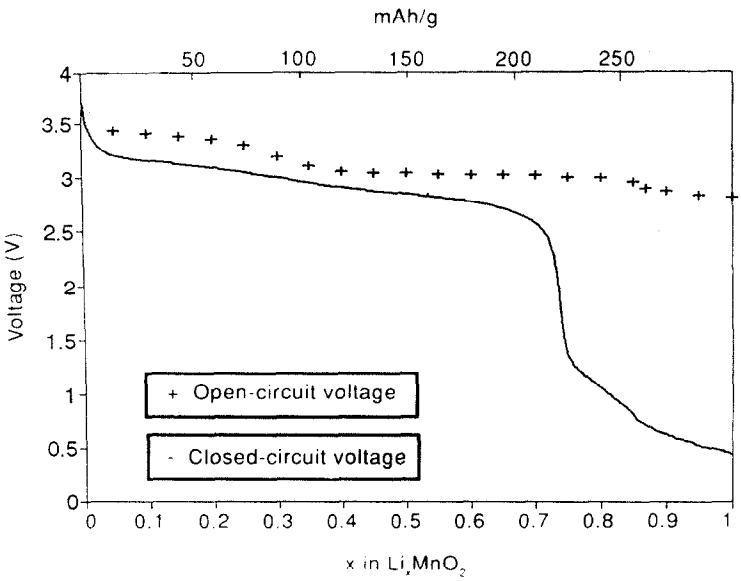

Fig. 7. Open-circuit voltage and closed-circuit voltage data for a Li/R-MnO_2 cell.

(iii) A broad peak at ~32° 2θ was attributed to unreacted Li in the form of Li_2CO_3 (or LiOH) that had formed as a result of the decomposition of $LiNO_3$ and the exposure of the decomposition product, Li_2O, to air. In the profile refinement, this peak did not coincide with the structure of either the lithiated R-MnO_2 phase or the spinel phase [20].

The MnO_2 framework structure of the lithiated R-MnO_2 phase (Fig. 6(c)) is remarkably similar to the structure obtained with n-butyllithium (Fig. 6(b)). In the latter case, lithiation induces a distortion of the hexagonally-close-packed oxygen layers at $Li_{\sim 0.25}MnO_2$ with a concomitant reduction of the manganese ions from +4 to +3. On the other hand, it is possible, in principle, that the distortion induced in R-MnO_2 by reaction with $LiNO_3$ at 300 °C may be achieved by the introduction of Li_2O into the R-MnO_2 framework without any change to the oxidation state of the manganese:

$$xLi_2O + \text{R-}MnO_2 \longrightarrow Li_{2x}MnO_{2+x}, \text{ where } 0 \leqslant x \leqslant 0.1 \quad (7)$$

It is worthwhile to note that in both types of reaction the distortion of R-MnO_2 is induced by only a small increase in the ratio of cations to anions in the structure. These data are consistent with reports that the reaction of CMD with $LiNO_3$ at 370 °C forms a product of approximate stoichiometry $Li_{0.2}MnO_2$ [16, 17]. Li and Pistoia [16] have also demonstrated that it is possible to oxidise $Li_{0.2}MnO_2$ by electrochemical extraction of Li; this process occurs on a short plateau at ~3.4 V (on closed circuit) versus a Li–Al alloy electrode which is in good agreement with our electrochemical OCV data for the Li/R-MnO_2 cell at the start of discharge (Fig. 7).

at 380 °C

When R-MnO_2 is reacted with $LiNO_3$ at 380 °C the X-ray diffraction pattern (Fig. 5(d)) is dominated by a lithiated R-MnO_2 phase ($a = 9.25$ Å, $b = 4.95$ Å, and $c = 2.85$ Å) and a cubic spinel phase with a lattice parameter $a = 8.15$ Å which falls

within the range of the lattice parameters of spinel phases reported for the $Li_2O \cdot yMnO_2$ ($2.5 \leqslant y \leqslant 4.0$) system [9]. If all the Li salt reacts with R-MnO_2, and the composition of the spinel is $Li_2Mn_4O_9$, the overall reaction (assuming fully-oxidised products) can be represented by:

$$3LiNO_3 + 7MnO_2 \longrightarrow 1.67Li_{0.2}MnO_{2.1} + 1.33Li_2Mn_4O_9 + 3NO_2 + 0.75O_2 \quad (8)$$

The predominance of a lithiated R-MnO_2 phase and the presence of unreacted Li salt in the 300 °C product (Fig. 5(c)), and the significant concentration of spinel and some residual unreacted Li salt in the 380 °C product (Fig. 5(d)) indicates that the reaction of R-MnO_2 with Li_2O progresses with increasing Li_2O concentration to form a series of $Li_2O \cdot yMnO_2$ structures with a decreasing value of y, according to the sequence:

$$\text{R-}MnO_2 \xrightarrow{Li_2O} Li_2O \cdot 10MnO_2(\gamma) \xrightarrow{Li_2O}$$

$$Li_2O \cdot (4.0\text{–}2.5)MnO_2(\text{spinel}) \xrightarrow{Li_2O} Li_2O \cdot MnO_2(\text{rock salt}) \quad (9)$$

With a homogeneous mixture and a Li:Mn ratio of 3:7 in the starting material, it is therefore unlikely that a Li-rich rock-salt phase is formed in any significant concentration in the lithiated R-MnO_2 products. The possibility of spinel compositions with $y > 4$ cannot be discounted. A typical X-ray diffraction pattern of a product obtained from the reaction of CMD with $LiNO_3$ at 370 °C (Li:Mn = 3:7) is given in Fig. 5(e) for comparison. It clearly shows the presence of the lithiated γ-MnO_2 phase and the spinel phase.

Composite dimensional manganese oxide (CDMO)

CDMO refers to a range of electrode materials initially developed by Sanyo Electric Co. for rechargeable Li battery applications [4, 23]. CDMO compounds with optimum electrochemical properties are prepared typically by the reaction of LiOH (or $LiNO_3$) and γ-MnO_2 at 370 °C using a Li:Mn ratio of 3:7 [18]. The powder X-ray diffraction pattern of these products has been interpreted in terms of a composite structure containing domains of γ-MnO_2 and Li_2MnO_3. However, because the powder X-ray diffraction pattern of Li_2MnO_3 can be confused with those of cubic-spinel phases in the $Li_2O \cdot yMnO_2$ system ($2.5 \leqslant y \leqslant 4.0$) and their cubic lithiated products, it is concluded from the foregoing discussion and following arguments that the spinel structure, not Li_2MnO_3, plays the dominant and vital role in stabilising CDMO electrodes and in contributing to their good electrochemical properties in rechargeable lithium cells:

(i) Spinels have thermodynamically-favoured structures in the Li–Mn–O system when synthesised at moderate temperatures, for example, 300–400 °C, particularly for compounds with Li:Mn ratios of 1:1.2 to 1:2.0. A Li:Mn ratio of 3:7 in the starting materials will therefore favour the formation of spinel components rather than Li_2MnO_3 which is Li-rich (Li:Mn ratio = 2:1).

(ii) Spinels are electrochemically-active and therefore contribute to the capacity of CDMO electrodes. Li_2MnO_3 is electrochemically inactive and in significant quantities will add 'dead weight' and reduce the capacity of the cathode.

(iii) Spinels offer three-dimensional pathways for Li^+ ion transport and therefore provide a route to the γ-MnO_2 domains of CDMO materials. By comparison, the low diffusion rate of Li^+ ions in the Li_2MnO_3 rock-salt structure at room temperature will reduce the rate at which the γ-MnO_2 domains can be utilised.

(iv) Spinels are mixed-valent compounds and will contribute to the electronic conductivity of the electrode during charge/discharge. Li_2MnO_3 is an electronic insulator

and will isolate regions of electroactive domains, thereby reducing the effectiveness of the electrode.

Finally, it is believed that the spinel component provides a cubic-close-packed oxygen ion array that stabilises the structure of the lithiated γ-phase during Li insertion/extraction reactions; removal of the spinel phase from the composite electrode would leave a lithiated γ-MnO_2 phase which on its own is expected, like a pure γ-MnO_2 electrode, to offer inferior cycling properties.

Conclusions

Significant progress has been made in synthesising high-purity MnO_2 materials and in understanding the structural features that account for their electrochemical properties in Li cells. Although more information about their long-term cycling performance is still required, it seems that α-MnO_2, spinel-related $Li_2O \cdot yMnO_2$ ($y \geqslant 2.5$) and stabilised γ-MnO_2 (CDMO) electrodes offer particular promise for 3 V rechargeable Li batteries.

References

1 E. Plichta, S. Slane, M. Uchiyama, M. Saloman, D. Chua, W. B. Ebner and H. W. Lin, *J. Electrochem. Soc., 136* (1989) 1865–1869.
2 J. R. Dahn, U. Von Sacken, M. W. Juzkow and H. Al-Janaby, *J. Electrochem. Soc., 138* (1991) 2207–2211.
3 J. M. Tarascon and D. Guyomard, *J. Electrochem. Soc., 138* (1991) 2864–2868.
4 T. Nohma. Y. Yamamoto, K. Nishio, I. Nakane and N. Furukawa, *J. Power Sources, 32* (1990) 373–379.
5 A. Lecerf, F. Lubin and M. Broussely, *US Patent No. 4 975 346* (1990).
6 M. H. Rossouw, D. C. Liles, M. M. Thackeray and W. I. F. David, *Mater. Res. Bull, 27* (1992) 221–230.
7 F. Lubin, A. Lecerf, M. Broussely and J. Labat, *J. Power Sources, 34* (1991) 161–173.
8 M. H. Rossouw and M. M. Thackeray, *Mater. Res. Bull., 26* (1991) 463–473.
9 M. M. Thackeray, A. de Kock, M. H. Rossouw, D. C. Liles, R. Bittihn and D. Hoge, *J. Electrochem. Soc., 139* (1992) 363–366.
10 A. F. Wells (ed.), in *Structural Inorganic Chemistry,* Clarendon Press, Oxford, 1975, pp. 459–460.
11 T. Ohzuku, M. Kitagawa and T. Hirai, *J. Electrochem. Soc., 137* (1990) 769–775.
12 M. M. Thackeray, W. I. F. David, P. G. Bruce and J. B. Goodenough, *Mater. Res. Bull., 18* (1983) 461–472.
13 M. M. Thackeray, K. Pearce and W. I. F. David, unpublished data.
14 A. de Kock, M. H. Rossouw, L. A. de Picciotto, M. M. Thackeray, W. I. F. David and R. M. Ibberson, *Mater. Res. Bull., 25* (1990) 657–664.
15 A. Mosbah, A. Verbaere and M. Tournoux, *Mater. Res. Bull., 18* (1983) 1375–1381.
16 L. Li and G. Pistoia, *Solid State Ionics, 47* (1991) 241–249.
17 M. Yoshio, S. Inoue, M. Hyakutake, G. Piao and H. Nakamura, *J. Power Sources, 34* (1991) 147–152.
18 L. Li and G. Pistoia, *Solid State Ionics, 47* (1991) 231–240.
19 M. M. Thackeray, A. de Kock, L. A. de Picciotto and G. Pistoia, *J. Power Sources, 26* (1989) 355–363.
20 M. M. Thackeray, M. H. Rossouw, D. C. Liles and R. J. Gummow, unpublished data.
21 JCPDS Powder X-ray Diffraction File: 39–375.
22 T. Ohzuku, M. Kitagawa and T. Hirai, *J. Electrochem. Soc., 136* (1989) 3169–3174.
23 T. Nohma, T. Saito, N. Furukawa and H. Ikeda, *J. Power Sources, 26* (1989) 389–396.